Facet-Dependent Intrinsic Activity of Single Co_3O_4 Nanoparticles for Oxygen Evolution Reaction

Zhibin Liu, Hatem M. A. Amin, Yuman Peng, Manuel Corva, Rossitza Pentcheva,* and Kristina Tschulik*

Deciphering the influence of nanocatalyst morphology on their catalytic activity in the oxygen evolution reaction (OER), the limiting reaction in water splitting process, is essential to develop highly active precious metal-free catalysts, yet poorly understood. The intrinsic OER activity of Co_3O_4 nanocubes and spheroids is probed at the single particle level to unravel the correlation between exposed facets, (001) vs. (111), and activity. Single cubes with predominant (001) facets show higher activity than multi-faceted spheroids. Density functional theory calculations of different terminations and reaction sites at (001) and (111) surfaces confirm the higher activity of the former, expressed in lower overpotentials. This is rationalized by a change in the active site from octahedral to tetrahedral Co and the potential-determining step from *OH to *O for the cases with lowest overpotentials at the (001) and (111) surfaces, respectively. This approach enables the identification of highly active facets to guide shape-selective syntheses of improved metal oxide nanocatalysts for water oxidation.

1. Introduction

The spinel Co_3O_4 has been widely reported as an active and low-cost catalyst toward the oxygen evolution reaction (OER), which is the sluggish anodic half-cell reaction of the water-splitting process.[1] Co_3O_4 materials can be synthesized in various shapes by morphological control, e.g. as spheres,[2] cubes,[3] sheets,[4] and wires.[5] In the pursuit of higher catalytic activities, these various shapes allowed to explore the possible correlations between crystal facets (e.g. (111), (001), (110), and (112)) and enhanced OER activity.[6] Extensive efforts have been exerted to identify the most active facet for OER on Co_3O_4.[7–9] However, experimentally quantifying and properly correlating the effect of exposed facets on OER activity, though important, is indeed a challenge due to the difficulty in selectively altering only this particle property (i.e., shape) while maintaining all others, e.g., sizes or capping agents of the synthesized particles. Previous attempts to synthesize and compare the activity of shape-controlled Co_3O_4 catalysts are summarized in Table S1 (Supporting Information). The existing literature shows a controversy, reporting different activity correlations of either (001) or (111) being the more active facet of Co_3O_4 toward catalyzing the OER.[7,10,11] None of the previous works, however, have fulfilled the criterion of having the same size, crystal structure and capping agent but distinctly different surface facet. This requisite is fulfilled in the present study ensuring that only one parameter, that is the exposed surface planes, is changed while convoluting effects of other nanoparticle properties are suppressed to a minimum. For example, in Ref. [10] the activity of four different crystal planes of Co_3O_4 were compared to explore their facet effects. However, these particles featured also different particle sizes (300 nm for cubes, 10 µm length for belts, 100–200 nm for octahedra and 8×4 µm sheets), prohibiting an unambiguous deconvolution of morphology effects from other contributions.[10] Additionally, the OER activity of Co_3O_4 measured on ensembles can be disturbed by many external factors,[12] e.g., the use of binders and conducting supports, different catalyst loadings and non-optimal iR corrections. Furthermore, during nanoparticle synthesis, exploitation of different capping agents[13] or reactant concentrations[9] is often required to obtain specific shapes. The contributions of such additives on catalyst properties (e.g., defect density[14]) and, hence, on the OER activity of nanocatalysts are yet unknown in most of the cases. Therefore, to get an in-depth understanding of the Co_3O_4 facet effect and establish intrinsic structure-activity relationships, a direct comparison is necessary that tries to avoid the external complexity

Z. Liu, H. M. A. Amin, M. Corva, K. Tschulik
Analytical Chemistry II
Faculty of Chemistry and Biochemistry
Ruhr University Bochum
44801 Bochum, Germany
E-mail: kristina.tschulik@rub.de
H. M. A. Amin
Chemistry Department
Faculty of Science
Cairo University
Giza 12613, Egypt
Y. Peng, R. Pentcheva
Theoretical Physics
Faculty of Physics and Center for Nanointegration (CENIDE)
University Duisburg-Essen
47057 Duisburg, Germany
E-mail: rossitza.pentcheva@uni-due.de
K. Tschulik
Max-Planck-Institut für Eisenforschung GmbH
Max-Planck-Straße 1, 40237 Düsseldorf, Germany

**ADVANCED
SCIENCE NEWS**
www.advancedsciencenews.com

**ADVANCED
FUNCTIONAL
MATERIALS**
www.afm-journal.de

in ensemble measurements and the uncontrolled intrinsic unknowns arising at the particles during different synthesis procedures.

To overcome ensemble limits, single-entity electrochemistry[15] has been applied in electrocatalysis to probe the intrinsic activity of nanoparticles (NPs) at the individual particle level.[4,16] Especially, the nano-impact approach is a powerful tool to assess the current response of individual NPs.[17] In a typical nano-impact measurement, a biased microelectrode is inserted into a suspension of NPs. Due to their Brownian motion, for example, particles can randomly collide with the microelectrode and establish electrical contact. Consequently, a perturbation in the measured current occurs, typically being spike-like in transformative or capacitive impacts or step-like in the case of catalytic nano-impacts. By quantitatively analyzing these current steps, information such as NPs size, aggregation behavior, electrical double-layer capacitance and catalytic reactivity can be extracted.[18] Recently, we demonstrated the use of the nano- impact method to evaluate the intrinsic OER activity of spherical $CoFe_2O_4$ NPs at the single particle level,[19] thereby ruling out external effects originating from ensemble studies using catalyst-binder composites.[20] Moreover, simulating the diffusional flux toward single nanocubes allowed for assessing their turnover frequencies and interference-free activities.[21]

Herein, this approach is applied to elucidate the influence of the surface-exposed crystal facet of a Co_3O_4 nanocatalyst on its OER activity. The correlation between surface properties and any measured electrocatalytic response is complex. Therefore, combining advanced experimental and theoretical studies is crucial to unravel the factors controlling the activity. In this aspect, DFT simulations can provide useful insights into the energetics of the intermediate steps and extract overpotentials for different surface orientations and terminations.[22] Additionally, the role of solvation and the surface coverage of the specific intermediates or reactants have been shown to have a major contribution on the OER activity.[23,24]

Considering these points, we herein investigate Co_3O_4 spheroids and cubes toward their OER catalytic activity. These particles were successfully synthesized with similar size, using the same reactants and capping agents. This crucially important prerequisite is not fulfilled in reported works on facet-dependence of OER performance (see Table S1, Supporting Information), making it difficult to separate morphology from other (simultaneously altered) catalyst properties like their size or surface terminating ligand. The very similar synthesis conditions used for both types of particles utilized herein, allow us to directly measure the influence of the surface-exposed Co_3O_4 facet on the OER performance of otherwise nearly identical catalysts. The activity of both types of Co_3O_4 NPs was probed at the ensemble level as well as at a single particle level. The electrocatalytic responses reveal the (001)-exposed cubes to show a better OER activity than spheroids (exposing both (001) and (111) facets). Furthermore, DFT calculations with a Hubbard U term (DFT + *U*) explore the OER activity at the (001) and (111) surfaces and indicate that overpotentials at the former are generally lower than at the latter, consistent with the experimental findings. Solvation contributions have also been included, and a range of possible terminations and reaction sites has been considered. For the majority of the different investigated crystal

terminations, either parallel to the (001) or (111) planes, the calculated energetics of the intermediate states and overpotentials support the (001) plane as the most active surface: For the (001) surface, the lowest overpotential is found to be 0.4–0.46 V, whereas for the (111) orientation the lowest value is 0.56 V.

2. Results and Discussion

The adopted synthesis methods for both Co_3O_4 spheroids and cubes have been designed to be as similar as possible, resulting in the successful synthesis of distinct shapes with similar particle sizes thanks to an identical precursor solution (Co^{2+} acetate) and capping agent (triethylene glycol, TEG). Details on the synthetic procedure are given in section SI-I (Supporting Information).

The obtained NPs are monodispersed, as shown in transmission electron microscopy (TEM) images and by the corresponding monomodal size distribution histograms (**Figure** 1a,b,e,f). Co_3O_4 cubes reveal an edge length of 8.7 ± 1.2 nm, while spheroids show an average diameter of about 9.6 ± 1.4 nm. Deduced from the selected area electron diffraction (SAED) patterns (Figure 1c), Co_3O_4 NPs exhibit a clear spinel structure (JCPDS no. 42-1467). Notably, high-resolution TEM (HR-TEM) images (Figure 1d) show that, while the Co_3O_4 cubes possess a well-defined shape, the nanometric spheroid particles are better modeled as complex polyhedra instead of perfect spheres. The resolved spheroid NPs expose both (001) and (111) facets on their surface (as derived from the 0.20 nm lattice fringe ascribed to the (400) plane). Thus, a model for this particle shape is presented in the inset of Figure 1d, which is a truncated octahedron possessing eight (111) and six (001) facets, matching well with the shape observed in HR-TEM bright-field imaging and consistent with previous reports.[25]

Further, the spheroidal and cubic nanoparticles were further characterized using X-ray diffraction (XRD), X-ray photoelectron spectroscopy (XPS), and Raman spectroscopy, see Supporting Information SI-III. The obtained data confirms that both particles only differ in the exposed crystal facets, but have the same crystal structure, capping agent, and very similar size. Thus, these samples are uniquely suited to identify facet-activity-correlations for OER catalysis at Co_3O_4 nanomaterials. This comparison of 8.7 nm sized cubes and 9.6 nm sized spheroids is expected to give valuable hints on the effect of different exposed facets on the OER activity, as the only major difference is ascribed to the presence of (111) facets on the spheroids. Firstly, classical rotating disc electrode (RDE) measurements were conducted on ensembles of NPs of both types. Additional details on the electrochemical measurements are presented in SI-II (Supporting Information). Linear sweep voltammetry (LSV) curves reveal that spheroids and cubes show similar OER current density responses without (Figure S1, Supporting Information) and with 95% iR-correction (**Figure 2**a). In Figure 2a, although the measured currents were normalized to the geometric area of the RDE electrode, as commonly adopted, and the same nominal amount has been drop-cast in each experiment, this comparison might still not be precise enough due to the difficulty in the determination of the real number of active sites involved in the OER process.[26]
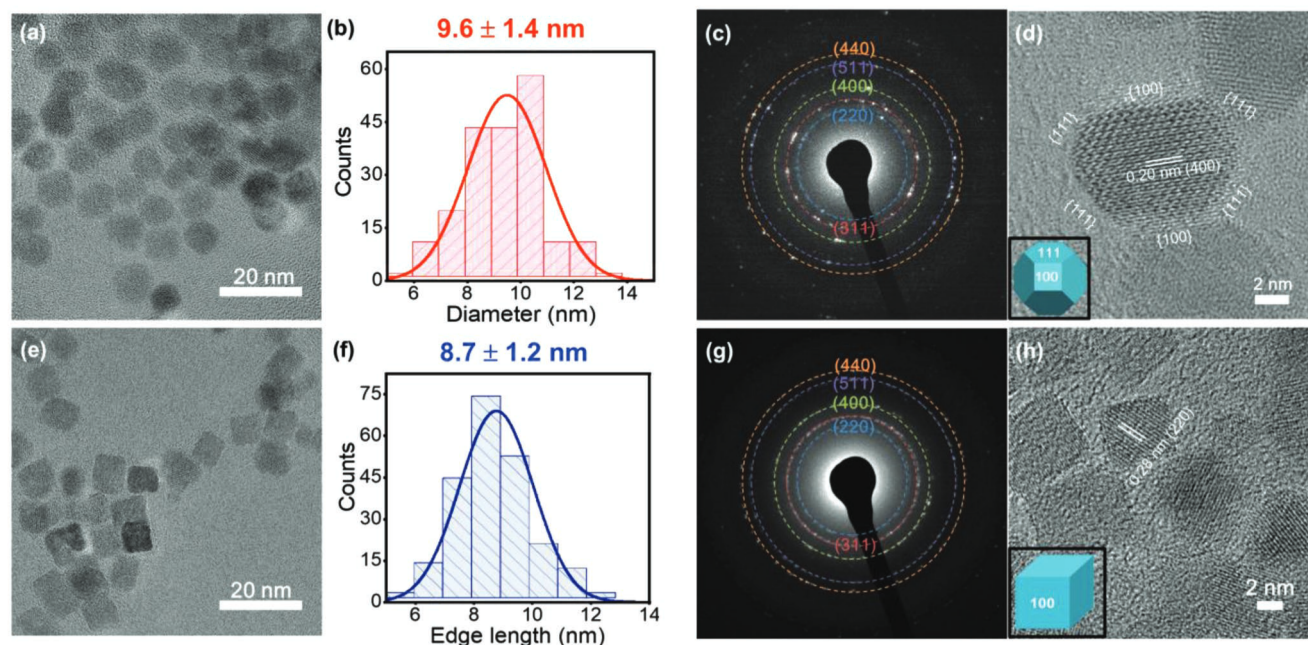
Figure 1. Spheroidal and cubic Co_3O_4 nanoparticles (upper and lower panels, respectively) are characterized by means of a,e) TEM, b,f) size distribution (mean diameter ± standard deviation), c,g) SAED pattern and d,h) HRTEM. The insets in (d) and (h) are a truncated octahedron and cube models, respectively.

Alternatively, the $Co^{3+/4+}$ oxidation peak may be used to roughly estimate the available Co atoms participating in the OER process.[27] Details about the evaluation of the exposed Co atoms are presented in section SI-IV (Supporting Information). The polarization curves were then normalized to the estimated number of exposed Co atoms. The obtained LSVs are shown in Figure 2b, and suggest a slightly higher activity of the cubes. Additionally, Tafel analysis shows slightly lower Tafel slope for the cubes than the spheroids (see Figure 2c,d), implying a possibly altered mechanism at different facets, as suggested also by the DFT results below and in agreement with previous reports.[11,13] In most of the previous ensemble studies, the opposite conclusion was drawn, that is the (111) are more active than (001) facets,[7,9,10,28] and thus, spheroids would be expected to be more active than cubes. This conflicting observation could be rationalized on the basis that previous works used different particle sizes for the different facets, which does not necessarily ensure the same activity trend. Nevertheless, only a very recent work reported the higher OER activity of (001) over (111) facet.[11] Hence, these measurements can easily be affected by other particle properties being altered simultaneously, such as the use of different capping agents and supports in these cases to get specific shape and size during NPs synthesis or even comparing shapes of different dimensions (see Table S1, Supporting Information). Additionally, to potentially probe the change of several properties at once, different catalyst wetting by the used binder or other ensemble effects might have added to the observed difference in activity in these studies. A table summarizing the starting materials, shapes, facets, sizes and activity parameters of different synthesized Co_3O_4 particles is shown in Table S1 (Supporting Information). Although it is challenging, we successfully managed to synthesize cubes and spheroid particles having the sa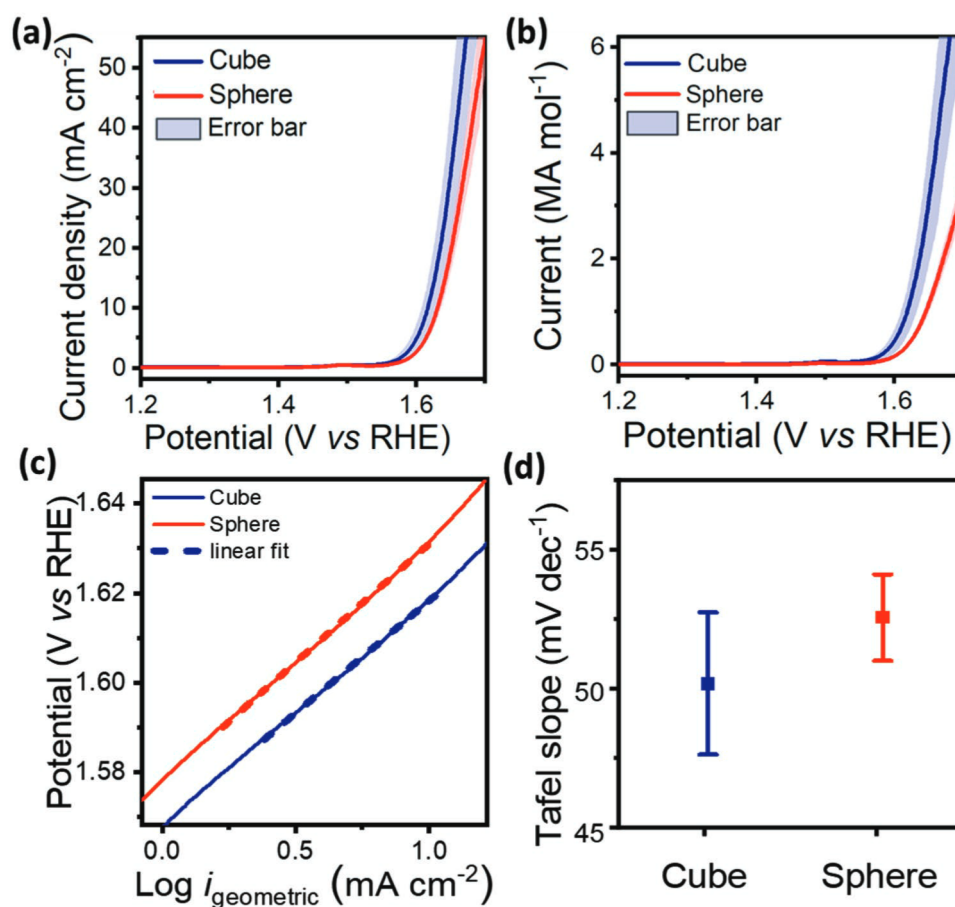me capping agent and the same diameter/edge length under nearly identical conditions, offering a proper assessment of the facet-dependent activity.

For the herein investigated particles, as the difference between the cubic and spherical particles nominally only lies in their shape, we further investigated the morphological stability of these particles. In particular, due to their well-defined edges, a possible shape transformation during OER might induce the nano cubes to adopt a more spherical shape, usually considered to be more energetically stable.[24,29] As this would result in nominally identical particles, it would also explain the very similar catalytic activity. Therefore, the nano cubes were characterized by HR-TEM after OER test (Figure S2, Supporting Information) and the images did not indicate changes in the cubic particle shape.

To discuss the minute difference between the two facets in Figure 2, the nature of the ensemble measurements can be considered. As detailed in many works investigating single entities, many external factors can affect the nanoparticle activity in ensemble studies.[12] Thus, nano-impact experiments were performed to enable a more reliable comparison of the intrinsic OER activity and to better correlate it to the respective particle geometry.

These single-particle experiments were carried out for Co_3O_4 spheroids by recording chronoamperograms at constant potentials in the range of 1.78–1.98 V vs RHE (0.8–1.0 V vs Ag/AgCl). Representative examples of the observed current steps for each potential are displayed in **Figure 3**a and more data for other potentials (Figure S3, Supporting Information) as well as for the Co_3O_4 cubes (Figure S4, Supporting Information) are presented. Obvious step-like signals are observed at 1.78 V and above. Furthermore, step current histograms at various potentials were established and fitted to get the corresponding mean values for the step currents, as displayed in Figure 3b. By

**ADVANCED
SCIENCE NEWS**

www.advancedsciencenews.com

**ADVANCED
FUNCTIONAL
MATERIALS**

www.afm-journal.de

Figure 2. LSV curves with 95% iR correction obtained in 0.1M KOH at 5 mV s^{-1} and 1600 rpm, normalized to a) the geometric area of the glassy carbon RDE and b) the moles of available Co atoms estimated from the Co$^{3+/4+}$ oxidation peak. Error bars represent the standard deviation of three independent measurements. The second normalization more clearly suggests an enhanced activity of the cubic particles. In addition, in (c) Tafel plots of the averaged dataset presented in (a) are compared and the resulting slope values are reported in (d). On the basis of this dataset, the cubic particles show slightly lower Tafel slopes, i.e. slightly faster kinetics.

plotting the step current versus the applied potential (**Figure 4**a), it is clearly seen that for both cubes and spheroids the step current increases slightly from 1.78 to 1.83 V, while a much higher value is obtained at 1.88 V. When the applied potential reaches 1.93 V, the step current reaches its maximum value and a plateau appears. This suggests that at 1.93 V, Co$_3$O$_4$ NPs reach the steady state condition.[19] The OER activity of spheroids and cubes measured by single-entity electrochemistry are compared and the result is summarized in Figure 4a. Although, the potential required to observe obvious current steps (1.78 V) and the potential to reach the steady state (1.93 V) are the same in both cases, the step currents of cubes are significantly higher than spheroids at various potentials, suggesting that cubes are more active than spheroids. This observation emphasizes the significance of the single particle measurement to reliably probe the facet effects. However, considering the different geometric surface areas (a sphere has a smaller surface area of ≈289 nm^2 than a cube of ≈378 nm^2 for 5 exposed faces, see section SI-V, Supporting Information), it is necessary to compare the current responses at low overpotentials in terms of step current densities to highlight kinetic effects that should not depend on mass-transport.

Due to the efficient mass transport at the nanosized particles (i.e. convergent rather than linear diffusion), the nano-impact approach achieves high current densities and steady-state step-like current response.[19,21] At low applied overpotentials, the particle surface area is relevant to evaluate the kinetics, while at high overpotentials the diffusional mass transport limits the reaction and a linear dependency of the steady state current on the particle radius or edge length is expected, see details in section SI-VI (Supporting Information). The step currents were, thus, normalized to the surface area of the NPs and are depicted in Figure 4b. After normalization, no clear differences can be observed at 1.78 and 1.83 V, while at 1.88 V (in the potential region of interest) a higher current density is obtained for cubes than spheroids. In fact, the diffusion limiting currents at a cube and a sphere of comparable sizes differ only marginally (≈2%),[21,30] as discussed in SI-VI (Supporting Information). Accordingly, the regions of steady state (1.93 and 1.98 V) should not be taken into consideration, as steady-state currents depend on the radius (edge length) of NPs (see Supporting Information).[31] To further test the validity of the results at 1.88 V, the two (for spheroids and for cubes) step-current datasets were randomly divided into three subsets
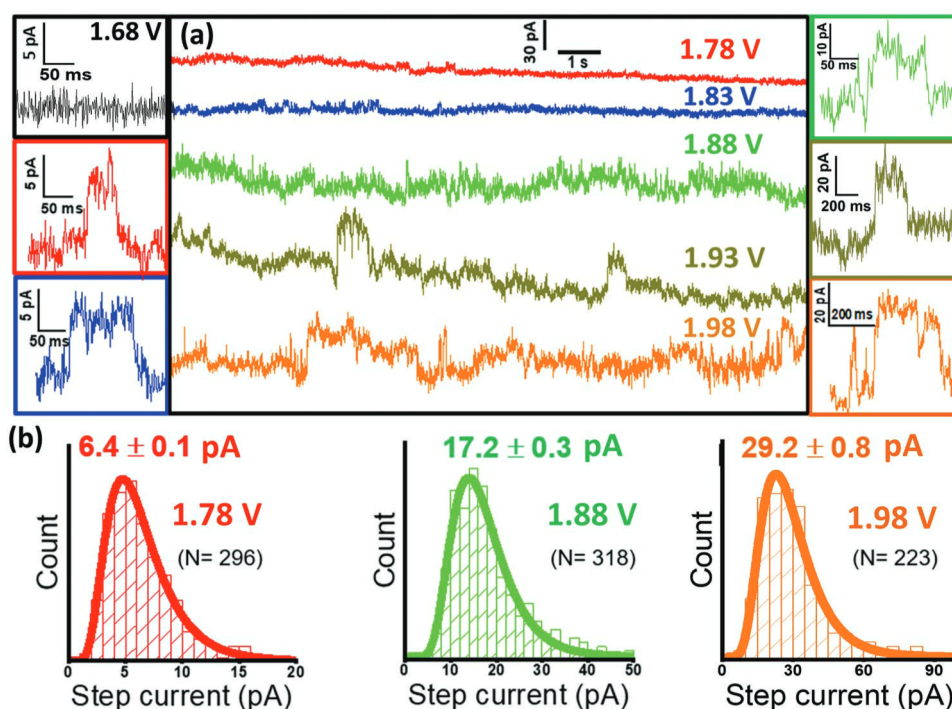
Figure 3. a) Representative current-time traces along with zoom-ins of a representative current step at various potentials (vs. RHE) and b) step current histograms (mean step heights ± standard errors and counting numbers of step peaks) of Co_3O_4 spheres at various potentials.

each and three novel and independent histograms were built and fitted (see Figure S4, Supporting Information). The mean value and standard deviation were calculated for the corresponding current densities, and the results are consistent with the previous estimate, that cubes show consistently higher step currents than spheroids.

To rationalize the detected influence of exposed facets on the intrinsic electrocatalytic activity, DFT+U calculations were performed to determine the energetics of OER intermediates and overpotentials at the Co_3O_4 (111) surface and to compare them to previous results for the (001) orientation.[23] While surface transformations of Co_3O_4 under OER operando conditions are reported to occur,[1] we assume that the above-considered terminations and sites still reflect the general reactivity trend. Details of the DFT+U calculations can be

found in SI-VII (Supporting Information). The bulk Co_3O_4 structure also showing the considered terminations for the two surface orientations is displayed in **Figure 5** and a top view of the studied terminations of the (111) surface is displayed in Figure S5 (Supporting Information). The reaction-free energies of OER intermediates and the resulting overpotentials at different terminations and reaction sites at the (001) and (111) surfaces of Co_3O_4 are shown in **Figure 6**a,b, respectively. The values are also listed in Table S2 (Supporting Information).

At the (001)-orientation both the B-layer with octahedral Co (Co^{Oct}) and oxygen and the A-layer with additional tetrahedral Co (Co^{Tet}) sites are considered (see Figure 5; Figure S5, Supporting Information), as well as different coverages with functional groups to describe the surface under applied voltage (for more details see Ref. [23]). Considering all these possibilities
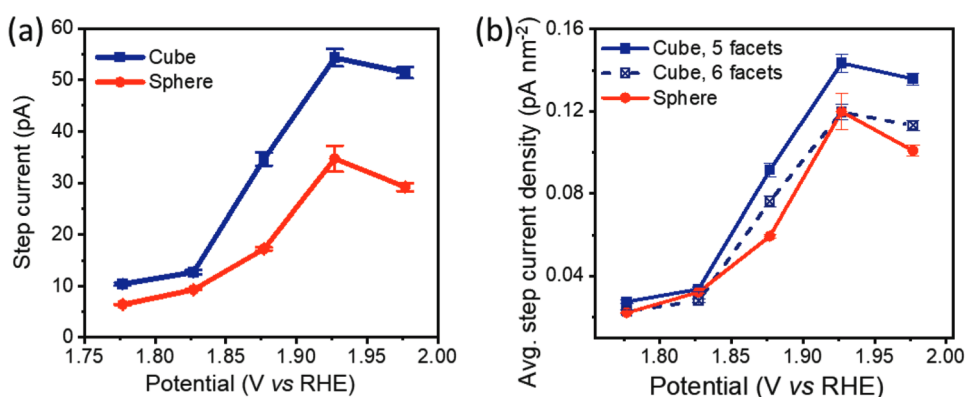
Figure 4. Comparisons of a) step currents and b) corresponding surface-normalized current densities of Co_3O_4 spheres and cubes at various potentials.
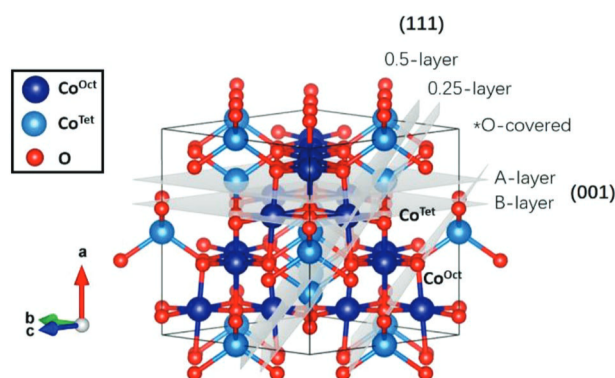
Figure 5. Bulk Co_3O_4 structure showing also the planes of the terminations considered for the (001) (A- and B-layer) and the (111)-surface orientations (0.25 ML, 0.5 ML and O-covered).

is a requirement for fair comparison of this complex system, where the energetics of each surface termination strongly depend on the environment condition (see Figure S6, Supporting Information). At the bare surface, the lowest overpotential is found for an octahedral Co reaction site at the B-layer (0.46 V), which is slightly higher if the surface is oxygenated (0.50 V). In contrast, for the A-layer the overpotential at an octahedral Co site is 0.63 V but is substantially reduced to 0.40 V for the oxygenated case. Concomitantly, the potential-determining step (PDS) switches from *OOH to *OH as in the B-termination. Regarding the (111) surface, terminations with a Co^{Tet} (0.25 ML) and with an additional Co^{Oct} (0.5 ML) were considered, as well as further coverage with oxygen or OH groups to model the surface under reaction conditions. At the (111) surface, the lowest overpotentials of 0.56 and 0.58 V are found for the Co^{Tet} site at the 0.25-layer and for the oxygenated surface, respectively, the PDS being in both cases the *OH deprotonation to *O. For the hydroxylated (111) surface, the overpotential rises to 0.70 V. Further cases with even higher overpotentials are shown in Figure S7 (Supporting Information) and listed in Table S2 (Supporting Information). Considering solvation effects with an implicit solvation model[32] leads generally to an increase of overpotential, which is more pronounced for the (001) surface and is associated with enhancement of binding energy.[23] However, the inclusion of

solvation does not change the PDS for all cases but the oxygenated surface.

Overall, the overpotentials for the (111) orientation tend to be higher than for the (001), consistent with the experimental finding. This trend is visible also in the volcano plot in **Figure 7**. The top of the ideal volcano stemming from the scaling relationship between ΔG_{*OH}^b and ΔG_{*OOH}^b[33] is reached for a binding energy difference of $\Delta G_{*OH}^b - \Delta G_{*OOH}^b \approx 1.7$ eV. Some of the calculated values, in particular for the (001) orientation, lie close or even above the volcano and toward the weak-binding leg of the volcano, indicating smaller deprotonation energies of *OH. Side views of the optimized structures of the OER intermediates on different reaction sites at the (001) and (111) facets along with the spin density are displayed in Figure 6 (further cases are shown in Figure S8 in the Supporting Information). The data indicate a strong variation of the magnetic moment at the Co reaction site at the B-layer termination between 2.1 μ_B for * and 0 μ_B for *OOH, indicating changes in the oxidation and spin state. This variation is significantly reduced at the A-layer (changes between 2.2–3.0 μ_B). Likewise, an enhanced fraction of Co^{2+} is found at the (111) surface (magnetic moment ~2.6 μ_B) for the octahedral sites, accounting for the observed higher activity of the (111) surface, in agreement with the electrochemical observation. At the 0.25 ML Co^{Tet} termination the subsurface octahedral layer acquires a magnetic moment of 1.0 μ_B, pointing to an intermediate spin state (compared to low spin state for Co^{3+} in bulk Co_3O_4).

3. Conclusion

In conclusion, the facet-dependent OER activity on spinel Co_3O_4 was successfully probed at the ensemble and single particle level by comparing the activity on spheroids ((001) and (111) facets) and cubes ((001) facets only). In contrast to the tentative differences in OER activity recorded on ensembles, the single particle studies unambiguously reveal that Co_3O_4 cubes are more active than spheroids when both NPs have otherwise identical parameters. DFT + U calculations confirm a higher OER activity of the (001) compared to the (111)-oriented Co_3O_4 surfaces. This may be attributed to the difference in the reaction site with lowest overpotential (octahedral vs tetrahedral)
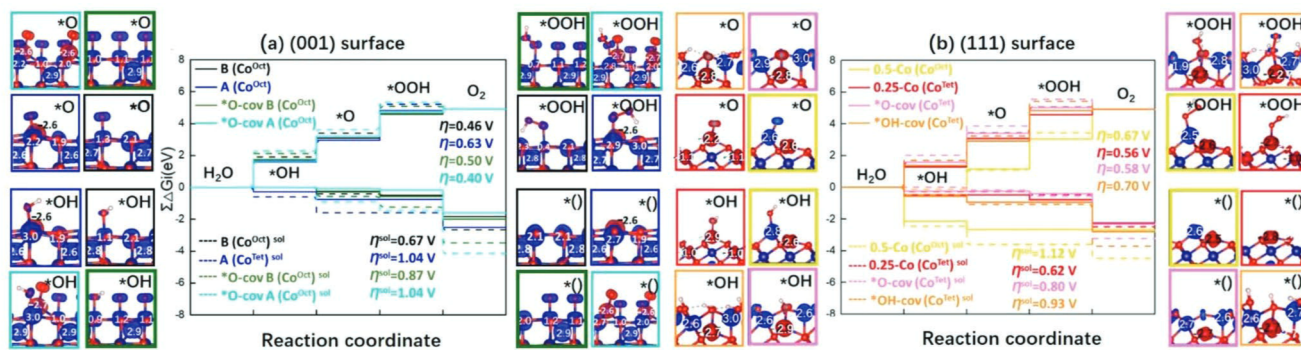
Figure 6. Cumulative free energies $\Sigma\Delta G_i$ of intermediates during OER for different terminations and reaction sites (in brackets) at a) the Co_3O_4 (001) surface (adapted from Ref. [23]), and b) Co_3O_4 (111). For (111) the four lowest overpotentials are shown (further cases are given in Figure S7, Supporting Information). The dashed lines indicate calculations including solvation effects.
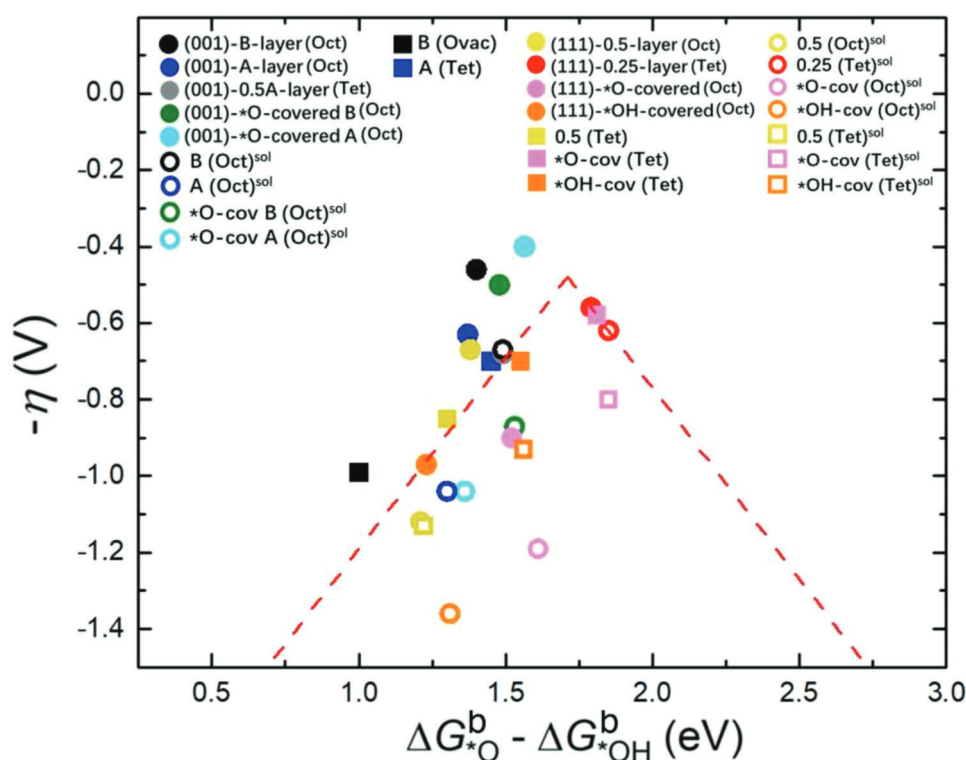
Figure 7. Volcano plot of the overpotential for both surface orientations as a function of the binding energy difference between *O and *OH intermediates. The dashed line is the ideal volcano from the scaling relationship of *OOH and *OH shown in Figure S9 (Supporting Information), the symbols are the calculated values for the different terminations and reaction sites.

and the change in potential determining step (*OH vs *O) for the (001) vs (111) surface and an enhanced fraction of Co^{2+} at the latter. This study provides both, new experimental and theoretical insights and a better understanding of the facet-dependent electrocatalytic activity. Hence, it highlights a promising novel approach for designing high-performance catalysts for energy conversion technologies via the selective synthesis of nanocatalysts with well-defined facets.

Supporting Information

Supporting Information is available from the Wiley Online Library or from the author.

Conflict of Interest

The authors declare no conflict of interest.

Data Availability Statement

The data that support the findings of this study are available from the corresponding author upon reasonable request.

[1] a) Z. Cai, Y. M. Bi, E. Y. Hu, W. Liu, N. Dwarica, Y. Tian, X. L. Li, Y. Kuang, Y. P. Li, X. Q. Yang, H. Wang, X. Sun, *Adv. Energy Mater.*

2018, *8*, 1701694. b) A. Bergmann, E. Martinez-Moreno, D. Teschner, P. Chernev, M. Gliech, J. F. de Araújo, T. Reier, H. Dau, P. Strasser, *Nat. Comm.* **2015**, *6*, 8625; c) L. Xu, Q. Q. Jiang, Z. H. Xiao, X. Y. Li, J. Huo, S. Y. Wang, L. M. Dai, *Angew. Chem., Int. Ed.* **2016**, *55*, 5277; d) H. M. A. Amin, H. Baltruschat, D. Wittmaier, K. A. Friedrich, *Elechtrochim. Acta* **2015**, *151*, 332; e) J. Huang, H. Sheng, R. D. Ross, J. Han, X. Wang, B. Song, S. Jin, *Nat. Chem.* **2021**, *12*, 3036; f) H. Y. Wang, S. F. Hung, H. Y. Chen, T. S. Chan, H. M. Chen, B. Liu, *J. Am. Chem. Soc.* **2016**, *138*, 36.

[2] Z. Liu, C. Yu, Y. Niu, X. Han, X. Tan, H. Huang, C. Zhao, S. Li, W. Guo, J. Qiu, *Carbon* **2018**, *140*, 17.

[3] L. Hu, Q. Peng, Y. Li, *J. Am. Chem. Soc.* **2008**, *130*, 16136.

[4] T. Quast, H. B. Aiyappa, S. Saddeler, P. Wilde, Y.-T. Chen, S. Schulz, W. Schuhmann, *Angew. Chem., Int. Ed.* **2021**, *60*, 3576.

[5] Y. G. Li, B. Tan, Y. Y. Wu, *Nano Lett.* **2008**, *8*, 265.

[6] a) T. Takashima, S. Hemmi, Q. Liu, H. Irie, *Cat. Sci. Technol.* **2020**, *10*, 3748; b) A. Govind Rajan, J. M. P. Martirez, E. A. Carter, *J. Am. Chem. Soc.* **2020**, *142*, 3600.

[7] Z. Chen, C. X. Kronawitter, B. E. Koel, *Phys. Chem. Chem. Phys.* **2015**, *17*, 29387.

[8] a) R. Gao, J. Zhu, X. Xiao, Z. Hu, J. Liu, X. Liu, *J. Phys. Chem. C* **2015**, *119*, 4516; b) K. Song, E. Cho, Y.-M. Kang, *ACS Catal.* **2015**, *5*, 5116.

[9] X. Han, G. He, Y. He, J. Zhang, X. Zheng, L. Li, C. Zhong, W. Hu, Y. Deng, T.-Y. Ma, *Adv. Energy Mater.* **2018**, *8*, 1702222.

[10] L. Liu, Z. Jiang, L. Fang, H. Xu, H. Zhang, X. Gu, Y. Wang, *ACS Appl. Mater. Interfaces* **2017**, *9*, 27736.

[11] L.-H. Zhang, H.-Y. Chuai, H. Liu, Q. Fan, S.-Y. Kuang, S. Zhang, X.-B. Ma, *J. Electrochem.* **2022**, *28*, 2108481.

[12] J. Masa, C. Andronescu, W. Schuhmann, *Angew. Chem., Int. Ed.* **2020**, *59*, 15298.

[13] S. Saddeler, U. Hagemann, S. Schulz, *Inorg. Chem.* **2020**, *59*, 10013.

[14] X. Li, X. Su, Y. Pei, J. Liu, X. Zheng, K. Tang, G. Guan, X. Hao, *J. Mater. Chem. A* **2019**, *7*, 10745.

[15] a) L. A. Baker, *J. Am. Chem. Soc.* **2018**, *140*, 15549; b) C. L. Bentley, M. Kang, P. R. Unwin, *J. Am. Chem. Soc.* **2019**, *141*, 2179; c) K. McKelvey, S. R. German, Y. L. Zhang, H. S. White, M. A. Edwards, *Curr. Opin. Electrochem.* **2017**, *6*, 4; d) F. T. Patrice, K. Qiu, Y.-L. Ying, Y.-T. Long, *Annu. Rev. Anal. Chem.* **2019**, *12*, 347.

[16] a) Y. Li, J. T. Cox, B. Zhang, *J. Am. Chem. Soc.* **2010**, *132*, 3047; b) Z. Jin, A. J. Bard, *Proc. Natl. Acad. Sci. USA* **2020**, *117*, 12651.

[17] a) R. Miao, L. Chen, L. Shao, B. Zhang, R. G. Compton, *Ang. Chem. Int. Ed.* **2019**, *58*, 12549; b) K. J. Stevenson, K. Tschulik, *Curr. Opin. Electrochem.* **2017**, *6*, 38.

[18] a) S. V. Sokolov, S. Eloul, E. Kätelhön, C. Batchelor-McAuley, R. G. Compton, *Phys. Chem. Chem. Phys.* **2017**, *19*, 28; b) M. Azimzadeh Sani, N. G. Pavlopoulos, S. Pezzotti, A. Serva, P. Cignoni, J. Linnemann, M. Salanne, M.-P. Gaigeot, K. Tschulik, *Angew. Chem., Int. Ed.* **2022**, *61*, 202112679.

[19] A. El Arrassi, Z. Liu, M. V. Evers, N. Blanc, G. Bendt, S. Saddeler, D. Tetzlaff, D. Pohl, C. Damm, S. Schulz, et al., *J. Am. Chem. Soc.* **2019**, *141*, 9197.

[20] N. Blanc, C. Rurainsky, K. Tschulik, *J. Electroanal. Chem.* **2020**, *872*, 114345.

[21] Z. Liu, M. Corva, H. M. A. Amin, N. Blanc, J. Linnemann, K. Tschulik, *Int. J. Mol. Sci.* **2021**, *22*, 13137.

[22] J. Chen, A. Selloni, *J. Phys. Chem. Lett.* **2012**, *3*, 2808.

[23] Y. Peng, H. Hajiyani, R. Pentcheva, *ACS Catal.* **2021**, *11*, 5601.

[24] a) J. Zhang, H. B. Tao, M. Kuang, H. B. Yang, W. Cai, Q. Yan, Q. Mao, B. Liu, *ACS Catal.* **2020**, *10*, 8597; b) F. T. Haase, A. Bergmann, T. E. Jones, J. Timoshenko, A. Herzog, H. S. Jeon, *Nat. Energy* **2022**, https://doi.org/10.1038/s41560-022-01083-w.

[25] X. Xie, Y. Li, Z.-Q. Liu, M. Haruta, W. Shen, *Nature* **2009**, *458*, 746.

[26] a) C. Wei, S. Sun, D. Mandler, X. Wang, S. Z. Qiao, Z. J. Xu, *Chem. Soc. Rev.* **2019**, *48*, 2518; b) H. M. A. Amin, H. Baltruschat, *Phys. Chem. Chem. Phys.* **2017**, *19*, 25527.

[27] S. Trasatti, O. A. Petrii, *J. Electroanal. Chem.* **1992**, *327*, 353.

[28] a) Q. Liu, Z. Chen, Z. Yan, Y. Wang, E. Wang, S. Wang, S. Wang, G. Sun, *ChemElectroChem* **2018**, *5*, 1080; b) B. Sidhureddy, J. S. Dondapati, A. Chen, *Chem. Comm.* **2019**, *55*, 3626.

[29] A. Bergmann, B. R. Cuenya, *ACS Catal.* **2019**, *9*, 10020.

[30] R. Wong, C. Batchelor-McAuley, M. Yang, R. G. Compton, *J. Electroanal. Chem.* **2021**, *903*, 115818.

[31] C. Batchelor-McAuley, R. G. Compton, *J. Electroanal. Chem.* **2020**, *877*, 114607.

[32] K. Mathew, R. Sundararaman, K. Letchworth-Weaver, T. A. Arias, R. G. Hennig, *J. Chem. Phys.* **2014**, *140*, 084106.

[33] a) I. C. Man, H.-Y. Su, F. Calle-Vallejo, H. A. Hansen, J. I. Martínez, N. G. Inoglu, J. Kitchin, T. F. Jaramillo, J. K. Nørskov, J. Rossmeisl, *ChemCatChem* **2011**, *3*, 1159; b) M. T. M. Koper, *J. Electroanal. Chem.* **2011**, *660*, 254.